



**HAL**  
open science

## **Nucleocapsid-specific and PD-L1+CXCR3+ CD8 polyfunctional T-cell abundances are associated with survival of critical SARS-CoV2-infected patients**

Lucille Adam, Pierre Rosenbaum, Paul Quentric, Christophe Parizot, Olivia Bonduelle, Noëlline Guillou, Aurélien Corneau, Karim Dorgham, Makoto Miyara, Charles-Edouard Luyt, et al.

### ► To cite this version:

Lucille Adam, Pierre Rosenbaum, Paul Quentric, Christophe Parizot, Olivia Bonduelle, et al.. Nucleocapsid-specific and PD-L1+CXCR3+ CD8 polyfunctional T-cell abundances are associated with survival of critical SARS-CoV2-infected patients. JCI Insight, 2021, 10.1172/jci.insight.151571 . hal-03984873v1

**HAL Id: hal-03984873**

**<https://hal.sorbonne-universite.fr/hal-03984873v1>**

Submitted on 21 Jul 2021 (v1), last revised 20 Mar 2023 (v2)

**HAL** is a multi-disciplinary open access archive for the deposit and dissemination of scientific research documents, whether they are published or not. The documents may come from teaching and research institutions in France or abroad, or from public or private research centers.

L'archive ouverte pluridisciplinaire **HAL**, est destinée au dépôt et à la diffusion de documents scientifiques de niveau recherche, publiés ou non, émanant des établissements d'enseignement et de recherche français ou étrangers, des laboratoires publics ou privés.

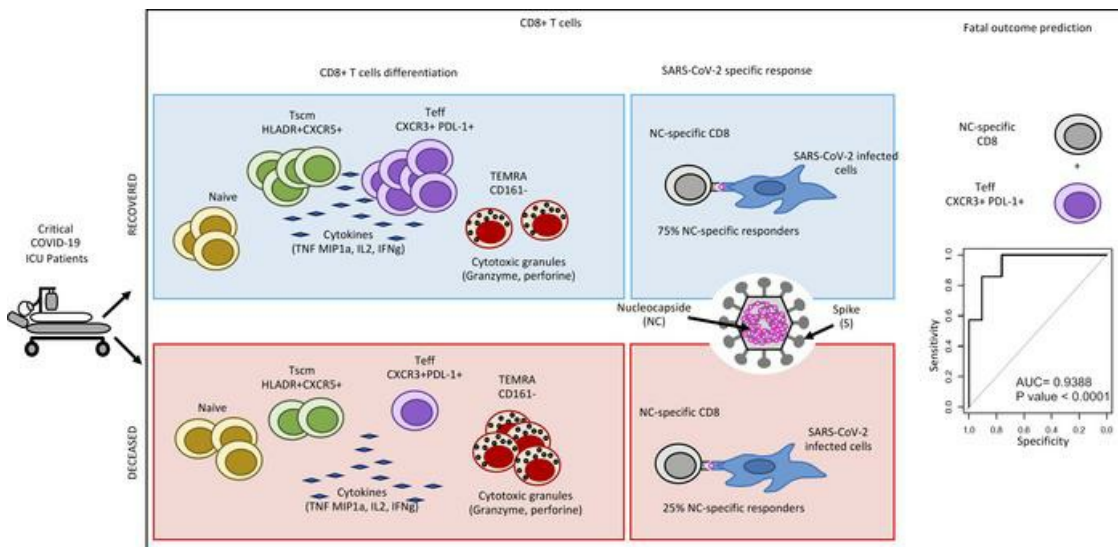
## Nucleocapsid-specific and PD-L1+CXCR3+ CD8 polyfunctional T-cell abundances are associated with survival of critical SARS-CoV2-infected patients

Lucille Adam, ... , Christophe Combadière, Behazine Combadière

JCI Insight. 2021. <https://doi.org/10.1172/jci.insight.151571>.

Research In-Press Preview Immunology

### Graphical abstract



Find the latest version:

<https://jci.me/151571/pdf>



1  
2 **Nucleocapsid-specific and PD-L1+CXCR3+ CD8 polyfunctional T-cell abundances are**  
3 **associated with survival of critical SARS-CoV2-infected patients**

4  
5 Lucille Adam<sup>1\*</sup>, Pierre Rosenbaum<sup>1\*</sup>, Paul Quentric<sup>1,2</sup>, Christophe Parizot<sup>1,2</sup>, Olivia  
6 Bonduelle<sup>1</sup>, Noëlline Guillou<sup>1</sup>, Aurélien Corneau<sup>3</sup>, Karim Dorgham<sup>1</sup>, Makoto Miyara<sup>1,2</sup>,  
7 Charles-Edouard-Luyt<sup>4,5</sup>, Amélie Guihot<sup>1,2</sup>, Guy Gorochov<sup>1,2</sup>, Christophe Combadière<sup>1\*\*</sup>, and  
8 Behazine Combadière<sup>1, \*\*+</sup>

9  
10 <sup>1</sup>Sorbonne Université, Inserm U1135, Centre d'Immunologie et des Maladies Infectieuses –  
11 Cimi-Paris, F-75013, Paris, France.

12 <sup>2</sup>Assistance Publique-Hôpitaux de Paris (AP-HP), Groupement Hospitalier Pitié-Salpêtrière,  
13 Département d'Immunologie, F-75013, Paris, France

14 <sup>3</sup>Sorbonne Université, UMS037, PASS, Plateforme de cytométrie de la Pitié-Salpêtrière  
15 CyPS, F-75013 Paris, France.

16 <sup>4</sup>Assistance Publique-Hôpitaux de Paris (AP-HP), Groupement Hospitalier Pitié-Salpêtrière,  
17 Service de Médecine Intensive–Réanimation et Pneumologie, F-75013, Paris, France

18 <sup>5</sup>Sorbonne Université, Inserm, Institute of Cardiometabolism and Nutrition (ICAN), Paris,  
19 France, F-75013, Paris, France

20  
21 **Footnotes**

22 \* LA and PR authors contributed equally to this work.

23 \*\* CC and BC are senior co-authors of this work

24  
25 ***Short title: Effector T cells in SARS-CoV-2 critical patient survival***

26  
27 **<sup>+</sup>Corresponding authors information**

28 Behazine Combadiere, PhD, Centre d'Immunologie et des Maladies Infectieuses (Cimi-  
29 Paris), Inserm, Sorbonne université, 91 Boulevard de l'Hôpital, 75013 Paris, France, e-mail:  
30 [behazine.combadiere@inserm.fr](mailto:behazine.combadiere@inserm.fr)

35

36 **Counts**

37 Title: 15 words

38 Abstract: 209 words

39 Manuscript text : approximatively 5 400 words

40 total word count: 7 800 words

41 Items: 5 Figures, 1 Table

42 Supplementary items: 3 figures + 2 tables

43

44

45

46 **List of abbreviations**

47 ARDS: Acute Respiratory Distress Syndrome; CyTOF: Cytometry by Time-of-flight Mass  
48 Spectrometry; ICU: Intensive Care Unit; t-SNE: t-distributed stochastic neighbour  
49 embedding

50

51 **Abstract**

52

53 **Rationale:** The importance of the adaptative T cell response in the control and resolution of  
54 viral infection has been well-established. However, the nature of T cell-mediated viral control  
55 mechanisms in life-threatening stages of COVID-19 has yet to be determined.

56 **Objective:** The aim of the present study was to determine the function and phenotype of T  
57 cell populations associated with survival or death of COVID-19 patients under intensive care  
58 as a result of phenotypic and functional profiling by mass cytometry.

59 **Findings:** Increased frequencies of circulating, polyfunctional, CD4<sup>+</sup>CXCR5<sup>+</sup>HLA-DR<sup>+</sup> stem  
60 cell memory T cells (T<sub>SCM</sub>) and decreased proportions of Granzyme-B and Perforin-  
61 expressing effector memory T cells (T<sub>EM</sub>) were detected in recovered and deceased patients,  
62 respectively. The higher abundance of polyfunctional CD8<sup>+</sup>PD-L1<sup>+</sup>CXCR3<sup>+</sup> T effector cells,  
63 CXCR5<sup>+</sup>HLA-DR<sup>+</sup> T<sub>SCM</sub>, as well as anti-nucleocapsid (NC) cytokine-producing T cells  
64 permitted to differentiate between recovered and deceased patients. The results from a  
65 principal component analysis showed an imbalance in the T cell compartment allowed for the  
66 separation of recovered and deceased patients. The paucity of circulating CD8<sup>+</sup>PD-  
67 L1<sup>+</sup>CXCR3<sup>+</sup> T<sub>eff</sub>-cells and NC-specific CD8<sup>+</sup> T-cells accurately forecasts fatal disease  
68 outcome.

69 **Conclusion:** This study provides insight into the nature of the T cell populations involved in  
70 the control of COVID-19 and therefor might impact T cell-based vaccine designs for this  
71 infectious disease.

72

73 **keywords:** COVID-19, T cells, differentiation, Sars-CoV-2, adaptive immunity

74

75

## 76 **Introduction**

77

78 The emergence of the new SARS-CoV-2-induced coronavirus disease 2019 (COVID 19)  
79 outbreak has rapidly emerged as an important healthcare, societal, and economic threat due to  
80 its extremely fast worldwide spreading and severity. In January 2021, more than 88 million  
81 cases and 1.9 million deaths have been reported (<https://covid19.who.int>). Even if the vast  
82 majority of cases are asymptomatic or characterized by mild symptoms (1, 2), 6% of SARS-  
83 CoV2-infected patients suffer from severe symptoms following the development of acute  
84 respiratory distress syndrome (ARDS) that can lead to death. Those severe to critical cases  
85 have a fatality rate of 2-8%, and require an admission in an intensive care unit (ICU) (3).  
86 During SARS-CoV-2 infection, numerous studies have pointed out a dysregulated and  
87 disruptive innate immune response inducing a general global hyperinflammation that leads to  
88 disease aggravation (4). This hyperinflammation has been associated with lung damage and  
89 ARDS with fatal outcomes. It is therefore reasonable to postulate that the inflammatory  
90 response measured both at cellular and molecular levels could represent a strong prognostic  
91 signature of the disease. Dysregulation of innate cell function and decreased production of  
92 type-I and III interferons have been highlighted as key contributors to viral persistence and  
93 disease severity (5, 6). However, decades of works on anti-viral T cell responses have  
94 underscored their essential role in viral clearance (7–9). Thus, we aimed at deciphering T cell  
95 differentiation and functional profiles during critical SARS-CoV-2 infection in ICUs.

96

97 SARS-CoV-2-specific CD4<sup>+</sup> and CD8<sup>+</sup> T cell responses have been described to be robustly  
98 induced in moderate to severely-ill COVID-19 patients (10–12). However, marked alterations  
99 in phenotypical and functional properties of SARS-CoV-2-specific T cells have been  
100 observed in severely ill patients compared to convalescent patients (12). During acute viral  
101 infection, viral peptides activate naïve T cell compartment initiating proliferation and  
102 differentiation of T cells into effector and memory cell subsets that participate to effective  
103 viral clearance (13–17). During severe SARS-CoV-2 infection, virus-specific CD4<sup>+</sup> T cells  
104 were found to be dominant over CD8<sup>+</sup> T cells with marked Th1-polarized CD4<sup>+</sup> T-cells  
105 specific for the viral Spike protein, although Th2 and Th17 cytokines were also detectable  
106 (18). Atypical T cell differentiation seems to occur in COVID-19 patients with T cells  
107 partially resembling Th1, Th2, Th17 and T follicular helper (Tfh) but lacking their principal  
108 feature including hyperactivation observed in the most severely ill patients (19). In addition,  
109 single-cell analyses of virus-specific CD4<sup>+</sup> T cells showed that their gene expression patterns

110 were distinct with disease severities (20). Strong memory CD4<sup>+</sup> and CD8<sup>+</sup> T-cells were  
111 induced in convalescent individuals following COVID-19 disease suggesting a role of T cell  
112 immunity in disease control (11), however the type of response favoring recovery or symptom  
113 worsen is yet to be determined.

114

115 For the past two decades, studies of T cell differentiation and functional markers have  
116 allowed to distinguish, naïve (CD45RA<sup>+</sup>CCR7<sup>+</sup>), activated, effector (T<sub>eff</sub>) (secretion of  
117 cytokines and cytolytic molecules). A fraction of these cells survives as memory T cells that  
118 contribute to long term immunity. These memory cells are subdivided central memory (T<sub>CM</sub>),  
119 effector memory (T<sub>EM</sub>) and stem cell memory T cells (T<sub>SCM</sub>) compartments, according to their  
120 phenotype CD45RA<sup>-</sup>CCR7<sup>-</sup>, CD45RA<sup>-</sup>CCR7<sup>+</sup> and CD45RA<sup>+</sup>CCR7<sup>+</sup>CD95<sup>+</sup> respectively  
121 (21, 22). In addition to surface markers defining differentiation of naïve into memory T cells,  
122 their homing capacities as well as the definition of exhaustion and inhibitory cell populations  
123 is changeable following acute and chronic infection (7, 22–24). Whereas effector memory T  
124 cells contribute to viral control, tissue homing capacities combined with cytotoxicity could  
125 induce tissue damage and accelerate mortality, whereas T cell-mediated viral clearance  
126 impedes disease exacerbation (25, 26). Thus, unbalanced in the disequilibrium between T cell  
127 subsets could be detrimental to viral control. During SARS-CoV-2 infection, a marked  
128 increase in terminally differentiated effector memory T cells (T<sub>EMRA</sub>) and effector memory T  
129 cells (T<sub>EM</sub>) as well as the concomitant decrease in the frequency of naïve CD8<sup>+</sup> cells has been  
130 observed (18). SARS-CoV-2 Specific CD4<sup>+</sup> T cells displayed major T<sub>CM</sub> phenotype while  
131 SARS-CoV-2 specific CD8<sup>+</sup> T are more heterogeneous with T<sub>EM</sub>, T<sub>EMRA</sub> (18) or T<sub>SCM</sub> and  
132 transitional memory phenotype (27). SARS-CoV-2-specific T cells are present relatively early  
133 and increase over time (18). It seems thus reasonable to hypothesize that quantitative and  
134 functional alteration of T cell compartment would affect disease outcome.

135

136 In our study, we used mass cytometry to decrypt phenotypic and functional profile of T cell  
137 responses from SARS-CoV-2 patients admitted in intensive care unit with or without fatal  
138 outcome. At approximately 15 days post-symptoms, we detected a higher abundance of  
139 multiple cytokine-producing CXCR5<sup>+</sup>HLA-DR<sup>+</sup> among CD4<sup>+</sup> T cells and NC-specific  
140 CD8<sup>+</sup> T-cells, CXCR5<sup>+</sup>HLA-DR<sup>+</sup> T<sub>SCM</sub>, as well as PDL-1<sup>+</sup>CXCR3<sup>+</sup>CD8<sup>+</sup> T<sub>eff</sub>-cells in  
141 patients who recovered from COVID-19. The paucity of PD-L1<sup>+</sup>CXCR3<sup>+</sup> T<sub>eff</sub>-cells and NC-  
142 specific CD8<sup>+</sup> T-cells was associated with a fatal disease outcome.

143

## 144 **Results**

145

### 146 **Skewed CD4<sup>+</sup> T cells in critical SARS-CoV-2 infection survival**

147

148 Fifty-six patients with confirmed SARS-CoV-2 infection were admitted in the Intensive Care  
149 Units (ICU) at a median of 9 days post symptoms (Table 1). In order to decipher the quality  
150 and intensity of adaptive immune responses in ICU patients who recovered and deceased  
151 ones, samples were analyzed for T cell responses as described in Figure 1A. Approximately  
152 one third of these patients deceased at a median of 21 days post-ICU admission. Two CyTOF  
153 panels (Supplementary Tables S1 and S2) were designed to study T cell phenotypes (n=42)  
154 and expression of effector molecules (n=21). In addition, SARS-CoV-2 peptide-specific  
155 cytokine-producing T cells were analyzed by flow cytometry (n=36). RBD (Receptor Binding  
156 Domain), Spike-subunits 1 (S1) and 2 (S2), NC-specific IgM, IgG, IgA were also measured in  
157 the serum (n=42).

158 Multiparametric mass cytometry staining helped to characterize CD4<sup>+</sup> T cell subsets using  
159 unsupervised analysis on panel #1 of 28 surface markers in 42 ICU patients (Supplementary  
160 table S1A). Visualization of t-distributed Stochastic Neighbor Embedding (viSNE  
161 implementation of t-SNE algorithm) of CD3<sup>+</sup>CD4<sup>+</sup> T cells (Figure 1B) using density plot  
162 revealed the distribution of several markers, including CCR7, CD45RA, CD127, CX3CR1,  
163 CXCR5, HLA-DR, FoxP3 and CD95, as depicted in Figure 1B. CCR7 and CD45RA mapping  
164 and indicated markers allowed to label T cells subsets according to the literature  
165 nomenclature as naïve, T<sub>EM</sub> and T<sub>CM</sub> (Supplementary Figure S1B). Seven major clusters were  
166 then defined and represented in t-SNE (Figure 1C). An additional heatmap (Figure 1D)  
167 allowed to visualize the level of expression of 16 major surface markers. According to these  
168 results, among CD3<sup>+</sup>CD4<sup>+</sup> T cells, we defined clusters of naïve  
169 (CCR7<sup>+</sup>CD45RA<sup>+</sup>CD127<sup>+</sup>CD27<sup>+</sup>), CXCR5<sup>+</sup>HLA-DR<sup>+</sup> T cells (CCR7<sup>+</sup>/intCD45RA<sup>+</sup> also  
170 expressing CD27, CXCR3, CD95 exhaustion markers PD1 and PDL-1), T reg (expressing  
171 FoxP3 and CD25), T<sub>EM</sub> CD127<sup>+</sup> (also expressing CX3CR1 and CD161), T<sub>EM</sub> CD127<sup>low</sup> and  
172 T<sub>EM</sub> CX3CR1<sup>+</sup> (also expressing CXCR3 and CD95). According to the literature,  
173 CXCR5<sup>+</sup>HLA-DR<sup>+</sup> T-cells might be T<sub>SCM</sub> because they share CCR7, CD45RA, CD27,  
174 CXCR3 and CD95 with T<sub>SCM</sub> described in HIV patients (22). Visualization of concatenated  
175 files in density plot according to recovered and deceased patients showed significant  
176 differential abundance of these clusters (Figure 1E). As shown in Radar chart and box plots  
177 (Figure 1F and G), we found that in deceased patients, naïve and T<sub>SCM</sub> CXCR5<sup>+</sup>HLA-DR<sup>+</sup> T-



178 cells were less abundant, whereas  $T_{EM}$   $CD127^{Low}$  were of higher frequencies however not  
179 significant (multiple Mann-Whitney test using Benjamini, Krieger, and Yekutieli false  
180 discovery rate (FDR) correction). These results revealed that an unbalanced  $CD4^+$  T cell  
181 differentiation, however not statistically significant, among recovered and deceased patients.

182

183

#### 184 **$CD4^+$ T-cell differentiation and functional profiles in critically infected COVID-19** 185 **patients.**

186

187 In order to evaluate the expression of effector molecules by  $CD3^+CD4^+$  T-cells, PBMCs  
188 (n=21) were incubated *in vitro* with brefeldin A for 16 hours prior staining using mass  
189 cytometry panel #2 (Supplementary Table S2). According to unsupervised FlowSOM  
190 analyses, we identified 9 clusters of  $CD3^+CD4^+$  T cells according to the expression of T cell  
191 differentiation surface markers, chemokine receptors and effector molecules (Figure 2).  
192 Figure 2A represents density plots of all nine clusters by t-SNE visualization. Several  
193 markers' intensities were represented in each density plot and could be mapped based on  
194 CCR7 and CD45RA expression. Additional representation of the mean expression of markers  
195 by a heatmap, allowed to overview the level of expression of these molecules (Figure 2B).  
196 We confirmed the identification of  $T_{SCM}$   $CXCR5^+HLA-DR^+$  previously observed in Figure  
197 1B when using our mass cytometry panel #2. Interestingly, these cells secreted a panel of  
198 cytokines such as MIP-1 $\beta$ , IFN $\gamma$ , IL-2 and activation/proliferation markers *i.e.* CD69, CD38,  
199 CD25 and Ki67 (Figure 1B). These results identify these cells as an important source of  
200 cytokine production.

201 We revealed additional subsets within  $T_{EM}$  and  $T_{CM}$  populations. Among  $T_{CM}$  ( $CCR7^+$   
202  $CD45RA^-$ ), we identified  $T_{CM}$  CRTH2,  $T_{CM}$  IL-5 $^+$  (Th2-like),  $T_{CM}$  "en route" (expressing  
203 CX3CR1, CCR6, CXCR6 and CXCR3, as major lung-homing receptors) and  $T_{CM}$  TNF $\alpha^+$   
204 cells (Figure 2A-B). Among the  $T_{EM}$  population, high levels of Granzyme-B and Perforin  
205 expression were observed and associated with CX3CR1 expression. These results suggest the  
206 capacity of cytotoxic  $T_{EM}$  to potentially migrate to inflammatory sites. As described in the  
207 literature, skewed T cell differentiation seems to occur in COVID-19 patients with modified  
208 proportion and phenotype of Th1, Th2, Th17 and T follicular helper (Tfh) (19).

209 Visualization of concatenated files in density plot according to recovered and deceased  
210 patients showed significant differential abundance of several clusters (Figure 2C).

211 Visualization of subpopulation abundances is shown in the radar chart (Figure 2D). ICU  
212 Patients who will recover, showed higher frequencies of naïve cells, T<sub>SCM</sub> CXCR5+HLA-  
213 DR+ however not significant after multiple Mann-Whitney test using Benjamini, Krieger, and  
214 Yekutieli FDR correction) with lower frequency of T<sub>EM</sub> however not significant.  
215 To better define anti-viral CD4 functions, we measured antigen-specific effector CD4+ T  
216 cells by intracellular cytokine staining (ICS) flow cytometry for IFN $\gamma$ , IL2 and/or TNF $\alpha$   
217 following *in vitro* stimulation with S1, S2, and NC overlapping 15-mers peptides (Figure 2E).  
218 S1-, S2-, and NC-specific CD4+ T-cells were heterogeneous among ICU patients (S1, S2  
219 n=46; NC n=39) (Figure 2E, left panel). Approximately 20% of patients who recovered did  
220 not display S1-, S2-, and NC-specific CD4+ T cells (non-responders) (Figure 2E, right panel).  
221 This proportion was approximately 30-40% in deceased patients. The ICS analysis showed  
222 mostly monofunctional (mainly IFN $\gamma$ +) and bifunctional responses (IFN $\gamma$ +TNF $\alpha$ ) (Figure  
223 2F). Although there was a tendency of higher frequency of non-responders to S1-, S2-, and  
224 NC-overlapping peptides in deceased patients, we did not observe any significant differences.  
225 Additional measurement of serum levels of RBD, S1, S2 and NC-specific IgM, IgG and IgA  
226 (Supplementary Figure S2A) did not allow to distinguish deceased from recovered patients  
227 (Supplementary Figure S2B).  
228 Therefore, CD4+ T-cell differentiation/functional profiles as well as antigen-specific CD4+ T  
229 cell responses showed marginal modification at the critical phase of SARS-CoV-2 infection.

230

231 **Surviving COVID-19 patients have increased levels of PDL-1+CXCR3+ CD8+ T<sub>eff</sub> and**  
232 **CXCR5+HLADR+ CD8+ T<sub>SCM</sub>.**

233

234 A similar approach was used to analyze CD3+CD8+ T cell differentiation and to determine  
235 their functional profile (Figure 1A and Supplementary Figure S1). According to unsupervised  
236 clustering and using density plot representation, we first observed the distribution of 15  
237 markers including CCR7, CD45RA, CXCR5, HLA-DR, CX3CR1, CXCR3, PDL-1, PD1,  
238 CD38 and CD161 as depicted in Figure 3A and 3B. CCR7 and CD45RA mapping and  
239 indicated markers allowed to label T cells subsets according to the literature nomenclature as  
240 naïve, T<sub>EM</sub>, T<sub>SCM</sub>, T<sub>CM</sub> and T<sub>EMRA</sub> cell subsets (Supplementary Figure S1). Seven major  
241 clusters were then defined and represented in a heatmap (Figure 3B). As represented in Figure  
242 3B, among CD3+CD8+ T cells, we defined clusters of cells as naïve  
243 (CCR7+CD45+CD127+CD27+) and CXCR5+HLA-DR+ CD8+ T- cells (CCR7+CD45RA+  
244 also expressing CD27, CD95, PDL-1, CD38 and caspase-3). According to the literature and

245 similar to CD4<sup>+</sup> T-cells, CD8<sup>+</sup> CXCR5<sup>+</sup>HLA-DR<sup>+</sup> T-cells shared CCR7, CD45RA, CD27,  
246 CXCR3 and CD95 with T<sub>SCM</sub> described in HIV patients (22). Among CD3<sup>+</sup>CD8<sup>+</sup> effector T  
247 cells, we identified T<sub>EM</sub> CX3CR1 (also expressing exhaustion markers PD-1, Caspase-3 and  
248 CD95) and a population of T<sub>eff</sub> PDL-1<sup>+</sup>CXCR3<sup>+</sup> that remains CCR7<sup>+</sup>CD45RA<sup>+</sup> and did not  
249 express CD95 (Figure 3B). T<sub>EMRA</sub> CD161<sup>+</sup> and CD161<sup>-</sup> CD8<sup>+</sup> T cells (CCR7<sup>-</sup> CD45<sup>int</sup> also  
250 expressing CX3CR1) as well as one subset of T<sub>CM</sub> were also identified. Visualization of  
251 concatenated files in density plot representation and according to recovered and deceased  
252 patients showed significant differential abundance of several clusters (Figure 3C). Statistical  
253 analyses were shown in radar charts and box plots (Figure 3D, 3E). Using multiple Mann-  
254 Whitney test with Benjamini, Krieger, and Yekutieli FDR correction, we showed that ICU  
255 patients who will recover have higher frequencies of naïve (adjusted *p-value* = 0.07), T<sub>SCM</sub>  
256 CXCR5<sup>+</sup>HLA-DR<sup>+</sup> (adjusted *p-value* = 0.07) with lower frequency of T<sub>EMRA</sub> CD161<sup>-</sup> (*p-*  
257 *value* <0.05). The main difference was observed in higher frequencies of T<sub>eff</sub> PDL-  
258 1<sup>+</sup>CXCR3<sup>+</sup> (adjusted *p-value* = 0.0006) in ICU patients who will recover. According to the  
259 literature, CXCR3<sup>+</sup> CD8<sup>+</sup> T cells has been identified as a biomarker that is associated with  
260 survival in melanoma patients with stage III disease (28) suggesting a potential role of this  
261 marker in SARS-CoV-2 infected patient survival.

262 In conclusion, similarly to the CD4<sup>+</sup> T-cell compartment, unbalanced differentiation of CD8<sup>+</sup>  
263 T cells distinguishes ICU patients who will recover or die in critical cases of SARS-CoV-2  
264 infection. We identified a subpopulation of CD8<sup>+</sup> T-cells expressing PDL-1<sup>+</sup>CXCR3<sup>+</sup> which  
265 was significantly under-represented in deceased patients and could have a potential role in  
266 disease control.

267

268

### 269 **Abundance of polyfunctional PDL-1<sup>+</sup>CXCR3<sup>+</sup> CD8<sup>+</sup> T cells and Nucleocapsid-specific** 270 **cytokine-producing T cells define survival versus fatal outcome following critical SARS-** 271 **CoV-2 infection**

272

273 In order to evaluate the expression of effector molecules by CD3<sup>+</sup>CD8<sup>+</sup> T-cells, PBMCs  
274 (n=21) were incubated *in vitro* with brefeldin A for 16 hours prior staining using mass  
275 cytometry panel #2 (Supplementary Table S2). According to unsupervised FlowSOM  
276 analysis, we identified 7 major clusters of CD3<sup>+</sup>CD8<sup>+</sup> T-cells assigning T cell differentiation  
277 surface markers, chemokine receptor and effector molecules expression (Figure 4). Figure 4A  
278 represents density plot of all 7 clusters using t-SNE visualization. Intensity and mapping of

279 several markers including CCR7 and CD45RA as well as chemokine receptors,  
280 activation/proliferation and differentiation markers are depicted in Figure 4A. Additional  
281 heatmap allowed to overview the level of expression of these molecules (Figure 4B). We  
282 confirmed the identification of 7 major clusters of CD3+CD8+ T -cells similar to Figure 3.  
283 Namely, naïve, T<sub>SCM</sub> CXCR5+HLA-DR+, T<sub>eff</sub> PDL-1+CXCR3+, T<sub>CM</sub>, T<sub>EMRA</sub> CD161+ and  
284 T<sub>EMRA</sub> CD161- populations were identified among CD3+CD8+ T-cells.  
285 Interestingly, T<sub>eff</sub> PDL-1+CXCR3+, remained the most polyfunctional cells with the highest  
286 production levels of multiple cytokines including MIP-1 $\beta$ , IFN $\gamma$ , IL-2 and TNF $\alpha$  followed by  
287 T<sub>SCM</sub> CXCR5+HLA-DR+ which also expressed MIP-1 $\beta$ , IFN $\gamma$ , IL-2, TNF $\alpha$  and also IFN $\alpha$ .  
288 These two subsets of CD8+ T -cells remains significantly higher in patients who survived as  
289 shown in the radar charts (Figure 4D). Their frequencies remained similar to the one  
290 observed in Figure 3E. T<sub>EM</sub> CX3CR1 CD8+ T-cells expressed lung homing markers,  
291 exhaustion markers PD-1 and cytotoxic molecules (Granzyme-B and Perforin). However,  
292 these expressions were lower compared to the T<sub>EMRA</sub> CD161+ cells as represented in the  
293 heatmap (Figure 4B). These results suggest that these two populations relatively of higher  
294 abundance in deceased patients might be harmful. T<sub>EMRA</sub> CD161 + also expressed CX3CR1 a  
295 homing marker to the lung suggesting a role of this population during SARS-CoV-2 infection.  
296 We also measured antigen-specific effector CD8+ T cells by intracellular cytokine staining  
297 (ICS) flow cytometry for (IFN $\gamma$ , IL2 and/or TNF $\alpha$ ) following *in vitro* stimulation with S1, S2,  
298 and NC-overlapping 15-mers peptides (Figure 4E-G). S1-, S2-, and NC-specific CD8+ T-  
299 cells were very heterogeneous among ICU patients (S1, S2 n=46; NC n=39). Approximately  
300 more than 50% of patients did not display Spike-specific CD8+ T cells (non-responders)  
301 (Figure 4E). Interestingly, the proportion of individuals without detectable NC-specific CD8+  
302 T cells was significantly higher in patients who deceased (73% non-responders) compared to  
303 patients who recovered (25% non-responders). The ICS analysis showed mostly  
304 monofunctional responses (mainly IFN $\gamma$ +) and bifunctional response (IFN $\gamma$ +TNF $\alpha$ ). The lack  
305 of NC-specific CD8+ T-cells was marked for all 3 functions tested.

306 Altogether, we showed that the low abundancy of polyfunctional T<sub>eff</sub> PDL-1+CXCR3+ and  
307 T<sub>SCM</sub> CXCR5+HLA-DR+ CD8+ T cells and the lack of NC-specific cytokine producing  
308 CD8+ T cells is one of the key features of patients with fatal outcome following critical  
309 SARS-CoV-2 infection.

310

311 **PD-L1+CXCR3+ and NC-specific CD8 T-cell frequencies predict fatal outcome of**  
312 **patients following critical SARS-CoV2 infection**

313

314 We used Principal Component Analysis (PCA) to visualize and to better understand the  
315 underlying structure of the data in an unsupervised way, by reducing multidimensional data  
316 sets in a two-dimension representation. It allows taking into account the similarities between  
317 subjects in order to have a robust informative viewpoint while preserving a high percent of  
318 the variation of the initial data set *i.e.* CD4+ and CD8+ T-cell subsets (n=42) (Figure 5A and  
319 B, respectively), and CD8+ T cells plus NC-specific CD8 T-cells (n=28) (Figure 5C). In  
320 figure 5A and 5B, the first two principal components allowed us to efficiently distinguish two  
321 groups as recovered and deceased patients. Analysis of CD4 and CD8 data set caught  
322 approximately 92 % and 75% of the variation of the initial information, thus allowing for  
323 conserving most information. We then added to the PCA analysis the information on NC-  
324 specific CD8 T cells (92 % data set used) to distinguishing recovered from deceased patients.  
325 Using PCA, we demonstrated that balance in T cell compartment during SARS-CoV-2  
326 infection allowed to differentially cluster patients who recovered from the one with fatal  
327 outcome. Among all sub-populations, the most significant changes were observed in T<sub>eff</sub> PD-  
328 L1+CXCR3+ and NC-specific CD8+ T-cells. Hence, we used logistic regression analysis to  
329 consider whether T<sub>eff</sub> PD-L1+CXCR3+ and NC-specific CD8+ T-cells might suppose the  
330 survival or fatal outcomes. The Receiver Operating Characteristics (ROC) curve showed that  
331 T<sub>eff</sub> PD-L1+CXCR3+ and NC-specific CD8 T-cells were the most accurate prognosticator of  
332 fatal outcomes (AUC=0.9354, *p value*<0.0001) (Figure 5D). As shown in Figure 5E, we  
333 segregated into two groups of COVID-19 deceased and recovered patients and compared their  
334 relative risk using a Cox proportional hazards model with other confounding factors including  
335 age, gender, hypertension (HT), obesity and the two main feature of adaptive T cell immune  
336 responses to the virus *i.e.* the proportion of NC-cytokine secreting CD8 T cells and T<sub>eff</sub>  
337 CXCR3+PDL-1+ CD8 T cells. Again, the lower abundance of NC-cytokine secreting CD8 T  
338 cells and T<sub>eff</sub> CXCR3+PDL-1+ CD8 T cells were at higher risk of death. The hazard ratio  
339 (Mantel-Haenszel) of NC-cytokine secreting CD8 T cells and T<sub>eff</sub> CXCR3+PDL-1+ CD8 T  
340 cells were of 14.9 and 12.2, respectively. The hazard ratio calculated for confounding factors  
341 such as age, smoking, obesity and HT, were not statistically significant using this model.  
342 In conclusion, these two parameters correctly foreseen survival or death prognostics of  
343 patients following critical SARS-CoV-2 infection reinforcing the important role of T cells  
344 during COVID-19 infection.

345  
346  
347  
348  
349  
350  
351  
352  
353  
354  
355  
356  
357  
358  
359  
360  
361  
362  
363  
364  
365  
366  
367  
368  
369  
370  
371  
372  
373  
374  
375  
376  
377

## Discussion

Our study is focused on the analysis of T cell responses in ICU patients in critical condition in order to decipher the role of T cells in acute viral SARS-CoV-2 infection. Although a humoral response was detected in all patients it did not allow to distinguish patients with fatal outcome. In contrast, a significant disequilibrium in the frequency of CD4<sup>+</sup> and CD8<sup>+</sup> subsets were found to be characteristic for patients who recovered or died during ICU hospitalization. Laing et al (29) have compared the immunological signature in asymptomatic/mild COVID-19 with that of healthy controls. It is evident that disorder in immune parameters could be major when comparing “disease” to “health” status. Laing et al (29) observed disproportionate depletions of CD4<sup>+</sup> Th17 and Th1 cells and T<sub>REG</sub> in COVID-19 patients compared to healthy adults. According to the literature, during SARS-CoV-2 infection increased proportion of cytotoxic follicular helper cells and cytotoxic Th cells (CD4-CTLs) responding to SARS-CoV-2 and reduced proportion of SARS-CoV-2-reactive T<sub>REG</sub> in hospitalized patients, as compared to those in the ICU (20).

In our study, the proportion of CD4<sup>+</sup> T-cell subsets was found to be significantly different with respect to disease outcome in severely infected patients when comparing deceased patients to recovered ones. We also observed that among CD4<sup>+</sup> T-cells, a higher abundance of naïve T-cells, polyfunctional T<sub>SCM</sub> CXCR5<sup>+</sup>HLA-DR<sup>+</sup> and lower abundance of T<sub>EM</sub> (effector memory) including those expressing Granzyme-B and Perforin were observed in patients who recovered. T<sub>SCM</sub> CXCR5<sup>+</sup>HLA-DR<sup>+</sup> shared T<sub>SCM</sub> markers such as CCR7, CD45RA, CD27, CXCR3 and CD95 described in HIV infection. Polyfunctionality of these cells in regard to major Th1 cytokine production (MIP-1 $\beta$ , IFN $\gamma$ , IL-2) and expression of activation/proliferation markers, *i.e.* CD69, CD38, CD25 and Ki67, suggests a potential central role in the control of infection. CD4<sup>+</sup> T<sub>SCM</sub> are efficiently induced following yellow fever vaccination and persist for decades (30). Different strategies have been explored to expand T<sub>SCM</sub> cells *in vitro* for tumor therapy because they can proliferate and survive vigorously under the continuous stimulation of tumor antigen (31). Inversely to T<sub>SCM</sub> up regulation in recovered patients, CX3CR1-expressing T<sub>EM</sub> were more abundant in deceased patients. The expression of chemokine receptors and cytotoxic molecules (Granzyme-B and



378 Perforin) by T<sub>EM</sub> suggest that they might migrate to tissue inflammation and induce damage,  
379 according to the literature (32).

380 The T<sub>CM</sub> subset expressed CXCR3<sup>+</sup> CX3CR1<sup>+</sup> CXCR6 and CCR6 which we named “en  
381 route” because of the high level of expression of multiple chemokine receptor. Among these  
382 homing receptors, CXCR6 is a chemokine receptor that allows cell homing to the lung.  
383 However, it has been shown in both tuberculosis and influenza mouse model that CXCR6  
384 deficiency did not affect the capacity of cells to migrate into the lung but was associated with  
385 an improved control of the infection (33). We also observed that SARS-CoV-2-specific CD4<sup>+</sup>  
386 T-cell responses, although undetectable in the blood of a fraction of ICU patients, did not  
387 allow to discriminate between recovered and deceased patients revealed.

388

389 Among CD8<sup>+</sup> T-cells, abundance of polyfunctional PD-L1<sup>+</sup>CXCR3<sup>+</sup> T-cells, and T<sub>SCM</sub>  
390 CXCR5<sup>+</sup>HLA-DR<sup>+</sup> and significantly higher responders to NC antigen, distinguished  
391 recovered from deceased patients. CXCR5<sup>+</sup>HLA-DR<sup>+</sup> CD8<sup>+</sup> T-cells population shared  
392 phenotypic profiles of T<sub>SCM</sub> as described in chronic viral infection as described in cancer and  
393 HIV (22). T<sub>SCM</sub> cells exhibit characteristics of conventional memory T cells. In Human  
394 Papilloma Virus (HPV) - associated cancer patients, CD8<sup>+</sup> T<sub>SCM</sub> were found to have long-  
395 term anti-tumor function both *in vivo* and *in vitro* (31). The T-cell receptor (TCR)  
396 rearrangement excision circles were similar in T<sub>CM</sub> and T<sub>EM</sub> suggesting that they have  
397 undergone multiple division (34). Of note, we also found Ki67 expression on T<sub>SCM</sub>  
398 CXCR5<sup>+</sup>HLADR<sup>+</sup> CD8<sup>+</sup> T-cells compared to other CD8 cell subsets from COVID-19  
399 patients. The role of these cells in infection has been shown to be more efficient than their  
400 CXCR5<sup>-</sup> counterpart for viral load control(35). T<sub>SCM</sub> have been detected in both CD4<sup>+</sup> and  
401 CD8<sup>+</sup> T-cell populations of mice (36) non-human primates and humans (37). They also have  
402 been proposed as a weapon in cancer immunotherapies. According to the literature and our  
403 observation of polyfunctionality of this population, we suggest that the T<sub>SCM</sub>  
404 CXCR5<sup>+</sup>HLADR<sup>+</sup> CD8<sup>+</sup> T-cells might have an importance for virus clearance in COVID-  
405 19.

406 Among CD8<sup>+</sup> T cells we also identified PD-L1<sup>+</sup>CXCR3<sup>+</sup> T-cells with polyfunctional  
407 cytokine profile producing MIP-1 $\beta$ , IFN $\gamma$ , IL-2 and TNF $\alpha$ . Increased IP-10 production  
408 induced by type-1 IFN in inflamed tissue could participate to the attraction of T<sub>eff</sub> PD-  
409 L1<sup>+</sup>CXCR3<sup>+</sup> CD8<sup>+</sup> cells and thus participate in viral control. Their presence in recovered  
410 patients compared with deceased patients could be a signature of viral control. According to  
411 the literature, the increased CXCR3<sup>+</sup> CD8<sup>+</sup> T cells has been identified as a biomarker that is

412 associated with survival in melanoma patients with stage III disease (28) suggesting a  
413 potential role of this marker in SARS-CoV-2 infected patient survival. In addition, a  
414 significant lower percentage of CD8<sup>+</sup> T-cell directed against NC were observed in deceased  
415 patients. Spike-specific CD8<sup>+</sup>T cells were detectable in deceased patients however lacked  
416 polyfunctionality. ROC analysis allowed to validate that the lack of PD-L1<sup>+</sup>CXCR3<sup>+</sup> T<sub>eff</sub> -  
417 cells and NC-specific CD8<sup>+</sup> T-cells correctly forecasts fatal disease outcome with a 93%  
418 accuracy.

419 The important role of memory T cells in the adaptive immune response to viral infections has  
420 been demonstrated (7, 38) and pointed out during COVID-19 infection either beneficial or  
421 detrimental with tissue damage (25). The potential protective role of NC-specific CD8<sup>+</sup> T cell  
422 responses could be of importance in future vaccine design (39). Indeed unlike spike protein,  
423 the internal NC protein is highly conserved among coronavirus strains, that might allow for a  
424 cross protection between strains, is abundantly expressed during infection and is highly  
425 immunogenic (40, 41). Indeed, spike protein is more likely to be subjected to a pressure of  
426 selection. We are facing the emergence of new SARS-CoV-2 variants originally discovered in  
427 Brazil, UK and South Africa with mutations on Spike protein which makes virus up to 71%  
428 more contagious (42). The strategy to use NC antigen in vaccine design could participate to  
429 the control of emerging SARS-CoV-2 variants. Further studies are necessary to evaluate the  
430 potential role of these cell populations as surrogate markers for viral control. Combining the  
431 knowledge from T cell immunology and induction of polyfunctional effector and memory  
432 cells will be beneficial for future vaccine design and its immunomonitoring.

433

434

435



## 436 **Materials and Methods**

437

### 438 ***Study participants***

439 A total of 56 adult patients with COVID-19 referred to the Department of Internal Medicine  
440 2, Department of Infectious Diseases and Intensive Care Units (ICU), Pitié Salpêtrière  
441 Hospital, Paris, were included in the study between March 2020 and May 2020. The diagnosis  
442 of COVID-19 relied on SARS-CoV-2 carriage in the nasopharyngeal swab, as confirmed by  
443 real-time reverse transcription-PCR analysis. Demographic and clinical characteristics are  
444 detailed in Table 1. One third of the patients deceased from COVID-19. Patient age ranged  
445 from 25 to 75 years old (median: 55 years, interquartile (IQ) range 48-62), with 12.7% of  
446 patients over 65 years old. Concerning immune traits, patients presented general  
447 lymphopenia, and granulocytosis, but no significant difference were observed between  
448 survivors and deceased. Delay between first symptoms appearance and ICU admission has  
449 been found to be homogeneous with a median at 9 days (interquartile range 7-9). Sampling  
450 was performed few days after admission (median: 6 days post admission, interquartile range:  
451 4-7 days after admission for specific T-cell responses measurement, and slightly before for  
452 cell phenotyping). The date of patient's decease after first symptoms onset were at a median  
453 of 21 days, (IQ:16-51). The interval between phenotyping and death is were at  $8 \pm 4$  days  
454 (median $\pm$ SEM) post-immunomonitoring antigen-specific T cell responses.

455

### 456 ***Study approval***

457 The study was conducted in accordance with the Declaration of Helsinki and the International  
458 Conference on Harmonization Good Clinical Practice guidelines and approved by the relevant  
459 regulatory and independent ethics committees. All patients gave informed consent. The study  
460 was registered and approved by local ethical committee of Sorbonne-Université/Assistance  
461 Publique-Hopitaux de Paris for ICU patients (N° CER-2020-31).

462

### 463 ***Blood sample preparation***

464 For all patients, whole blood was collected in acid citrate dextrose tubes. Peripheral blood  
465 mononuclear cells (PBMCs) were isolated by density-gradient sedimentation using  
466 Lymphocyte separation medium (Eurobio, France). Isolated PBMC were cryopreserved in  
467 fetal bovine serum (FBS) (Dutscher, France) containing 10 % DMSO and stored at  $-150^{\circ}\text{C}$ .  
468 PBMCs were used for measurement of SARS-CoV-2 antigen-specific T cells and mass

469 spectrometry staining. Serum was prepared from whole blood collected in tube without  
470 coagulant, and stored at -80°C for anti-SARS-COV-2 antibody measurement.

471

#### 472 ***Serum antibody dosage***

473 The presence of serum antibodies, specific for viral antigen was determined with the  
474 Maverick™ SARS-CoV-2 Multi-Antigen Serology Panel (Genalyte Inc. USA), according to  
475 the manufacturer's instructions. This technology has been designed to detect antibodies  
476 specific for the five SARS-CoV-2 antigens, nucleocapsid, Spike RBD, full length spike  
477 S1+S2, Spike S1 and Spike S2 subunits, immobilized on a chip, within a multiplex format  
478 based on photonic ring resonance technology. It detects and measures changes in resonance  
479 when antibodies bind to their respective antigens. Threshold values for positivity were set by  
480 the manufacturer (43, 44).

481

#### 482 ***Antigen-specific T cells and Intracellular staining (ICS)***

483 PepMIX SARS-CoV-2 peptide pools (JPT peptide technologies, Berlin, Germany)  
484 corresponding to 15-mer overlapping peptides of the nucleocapsid (NC, 102 peptides), the  
485 Spike subunit 1 (S1, 157 peptides) and Spike subunit 2 (S2, 158 peptides) were used to  
486 measure SARS-CoV-2-specific T cell responses. PBMCs were thawed and then rest for 5h  
487 hours in complete medium (RPMI 1640 medium added with 10% Bovine serum (Dutscher,  
488 France), 1% L-glutamine, 1% streptomycin/neomycin, 1% sodium pyruvate and 1% non-  
489 essential amino acid; Gibco). After resting, cells were washed and distributed in 96 round  
490 bottom-well plate. Stimulation was performed with 1.5 µg/ml of S1-, S2- or NC-peptide  
491 pools. Medium containing DMSO was used as unstimulated control, and human Dynabeads  
492 CD3/CD28 (Gibco, France) was used for positive control. After 1h, brefeldin A (Sigma,  
493 France) was added at a final concentration of 10 µg/ml. Cells were cultured for additional  
494 15h, before flow cytometry ICS as follow: live and dead staining was performed using  
495 live/dead fixable kit (Molecular Probes), followed by surface staining at 4°C using anti-CD3-  
496 APC-H7 (Clone SP 34-2), anti-CD8-FITC (Clone SK1) antibodies (BD Biosciences, France)  
497 and anti-CD4 BV650 (Clone OKT4) (Biolegend, France). PBMCs were then washed and  
498 fixed using the Fixation/permeabilization kit solution (BD Biosciences). Anti-TNFα-PE-Cy7  
499 (MAb11), IFNγ-AF700 (Clone B27), CD3-APC-H7 (Clone SP 34-2) (BD Biosciences,  
500 France), and anti-IL-2-APC (Clone N7.48 A) (Miltenyi Biotec, France) were used for  
501 intracellular staining. Cells were then washed and were performed on Fortessa X20 (BD

502 Biosciences, USA). Live events were analyzed by Boolean combination gating with FlowJo  
503 software (Tree Star Inc., USA). Background cytokine responses detected in negative controls  
504 were subtracted from those detected in stimulated samples.

505

### 506 ***Mass cytometer staining***

507 For the PBMCs phenotyping panel #1 (Supplementary Table S1), cells were thawed and let to  
508 rest during 1h in complete medium. For the PBMCs functional characterization panel #2  
509 (Supplementary Table S2), PBMC were thawed and let to rest for 5h hours in complete  
510 medium, before Brefeldin A (10µg/ml) was added for an overnight incubation. Five to ten  
511 million of PBMC were used for the staining. Cell viability was evaluated with a Cisplatin  
512 staining (Fluidigm, Inc) before blocking unspecific staining with Human Fc block (BD). After  
513 surface staining, cells were washed with Maxpar cell staining buffer (Fluidigm, France) and  
514 then fixed and permeabilized with the Transcription Factor buffer set (BD). PBMC were  
515 resuspended in heparin solution before the addition of the intracellular antibody mix. Finally,  
516 Iridium staining was performed in PBS 2% PFA at 4°C overnight. Cells were then kept at  
517 80°C during one to three weeks. After thawing, cells stained PBMCs were consecutively  
518 washed with PBS, Maxpar Cell Acquisition Solution (Fluidigm), and deionized water.  
519 Calibration beads in EDTA (Fluidigm) were added before the acquisition with a Helios at the  
520 “plateforme de cytométrie de la Pitié-Salpetriere (CyPS)”.

521

### 522 ***Mass cytometry analysis***

523 After sample acquisition, data from each sample were normalized (Mass cytometer. software  
524 version 6.7.1014 (Fluidigm). A quality control step consisting in checking number of cell  
525 events and marker signal in comparison with an internal control was then performed. Data  
526 were then cleaned based on beads, Barium/Cesium contamination, doublet and dead cell  
527 removal to keep only CD45+ cells. CD3+CD4+ T cells and CD3+CD8+ T cells  
528 (Supplementary Figure S1A) were selected prior analysis using OMIQ  
529 (<https://www.omic.ai/>). FlowSOM algorithm allowed automatically split CD4+ T cell and  
530 CD8+ T cells population into major clusters identified in regard to CCR7 and CD45RA  
531 (Supplementary Figure 1B). Cell cluster were labeled based on CD45RA/CCR7 expression.  
532 OMIQ platform was used to display Opt-SNE, FlowSOM analyses and heatmap  
533 representations.

534

535

536 ***Statistical analyses***

537 Principal Component Analysis (PCA), Radar and Receiving operator characteristic (ROC)  
538 curve were respectively performed using FactoMiner/FactoExtra, fmsb and pROC R  
539 packages. Combination of multiple parameters and (Area under curve) AUC determination  
540 for the ROC models were performed by binomial generalized linear model. Mann-Whitney  
541 tests were used when comparing abundance of cell populations in deceased versus recovered  
542 patients. Adjusted p-values for multiple Mann Whitney test procedures were generated  
543 including Benjamini, Krieger, and Yekutieli procedures for the control of the false discovery  
544 rate (FDR). Corrected p-values less than 0.05 were considered to indicate statistical  
545 significance. Statistical analyses and graph representation were performed using either  
546 GraphPad Prism 9 Software or R.

547

548

549

550 **Acknowledgments**

551 We thank the patients that agreed to participate in this study and all health-care workers  
552 involved in the diagnosis and treatment of patients of Assistance Publique Hôpitaux de Paris  
553 (AP-HP), intensive care unit and the immunology department staff members. We also thank  
554 the administrative staff at the Research and Innovation office (Mrs Laura Wakselman) of  
555 Pitié-Salpêtrière Hospital for their support.

556  
557 **Author contributions**

558 BC and CC designed the study, PR and LA designed and performed flow cytometry and mass  
559 cytometry experiments with the support of AC and NG. CP and MM performed antibody  
560 dosage. LA flow cytometry analysis, BC and PR performed mass-cytometry data analyses.  
561 PR, LA, KD, CP, OB participated to bio-banking. PQ was responsible for clinical data mining  
562 and analysis. MM, CEL, GG and AG provided patient sample access. BC and CC provided  
563 financial support. BC, CC, LA and PR wrote the manuscript. All authors contributed in  
564 reviewing the manuscript.

565  
566 **Conflict of interest statement**

567 The authors declare no conflict of interest regarding the publication of this work.

568  
569  
570 **Funding**

571 The study was supported by Fondation de France, « Tous unis contre le virus » framework  
572 Alliance (Fondation de France, AP-HP, Institut Pasteur) in collaboration with Agence  
573 Nationale de la Recherche (ANR Flash COVID19 program), and by the SARS-CoV-2  
574 Program of the Faculty of Medicine from Sorbonne University (I-COVID programs). BC  
575 laboratory is supported by grants from AG2R LA MONDIALE (Region IDF, France),  
576 Fondation pour la Recherche Médicale (FRM) team award. LA and PR are recipient of post-  
577 doctoral fellowships from the European Union's Horizon 2020 Research and Innovation  
578 Programme under grant agreement No. 681137 and ANR Flash COVID19 program.

579  
580  
581  
582  
583

584 **References**

585

- 586 1. Huang C, et al. Clinical features of patients infected with 2019 novel coronavirus in  
587 Wuhan, China.. *Lancet Lond. Engl.* 2020;395(10223):497–506.
- 588 2. Chen G, et al. Clinical and immunological features of severe and moderate coronavirus  
589 disease 2019. *J. Clin. Invest.* 2020;130(5):2620–2629.
- 590 3. Verity R, et al. Estimates of the severity of coronavirus disease 2019: a model-based  
591 analysis.. *Lancet Infect. Dis.* 2020;20(6):669–677.
- 592 4. Pedersen SF, Ho Y-C. SARS-CoV-2: a storm is raging. *J. Clin. Invest.* 2020;130(5):2202–  
593 2205.
- 594 5. Wen W, et al. Immune cell profiling of COVID-19 patients in the recovery stage by single-  
595 cell sequencing. *Cell Discov.* 2020;6(1). doi:10.1038/s41421-020-0168-9
- 596 6. Hadjadj J, et al. Impaired type I interferon activity and inflammatory responses in severe  
597 COVID-19 patients . *Science* 2020;eabc6027.
- 598 7. Wherry EJ, et al. Molecular Signature of CD8+ T Cell Exhaustion during Chronic Viral  
599 Infection. *Immunity* 2007;27(4):670–684.
- 600 8. Wherry EJ. T cell exhaustion . *Nat. Immunol.* 2011;12(6):492–499.
- 601 9. Chen Z, John Wherry E. T cell responses in patients with COVID-19 . *Nat. Rev. Immunol.*  
602 2020;20(9):529–536.
- 603 10. Grifoni A, et al. Targets of T Cell Responses to SARS-CoV-2 Coronavirus in Humans  
604 with COVID-19 Disease and Unexposed Individuals. *Cell* [published online ahead of print:  
605 May 2020]; doi:10.1016/j.cell.2020.05.015
- 606 11. Peng Y, et al. Broad and strong memory CD4+ and CD8+ T cells induced by SARS-CoV-  
607 2 in UK convalescent individuals following COVID-19. *Nat. Immunol.* [published online  
608 ahead of print: September 4, 2020]; doi:10.1038/s41590-020-0782-6
- 609 12. Schub D, et al. High levels of SARS-CoV-2–specific T cells with restricted functionality  
610 in severe courses of COVID-19. *JCI Insight* 2020;5(20):e142167.
- 611 13. Flynn KJ, et al. Virus-Specific CD8+ T Cells in Primary and Secondary Influenza  
612 Pneumonia. *Immunity* 1998;8(6):683–691.
- 613 14. Kaech SM, Cui W. Transcriptional control of effector and memory CD8+ T cell  
614 differentiation. *Nat. Rev. Immunol.* 2012;12(11):749–761.
- 615 15. La Gruta NL, Turner SJ. T cell mediated immunity to influenza: mechanisms of viral  
616 control. *Trends Immunol.* 2014;35(8):396–402.
- 617 16. Ahmed R, et al. Protective immunity and susceptibility to infectious diseases: lessons

618 from the 1918 influenza pandemic. *Nat. Immunol.* 2007;8(11):1188–1193.

619 17. Ahmed SF, et al. Preliminary Identification of Potential Vaccine Targets for the COVID-  
620 19 Coronavirus (SARS-CoV-2) Based on SARS-CoV Immunological Studies. *Viruses*  
621 2020;12(3):254.

622 18. Weiskopf D, et al. Phenotype and kinetics of SARS-CoV-2-specific T cells in COVID-19  
623 patients with acute respiratory distress syndrome. *Sci. Immunol.* 2020;5(48):eabd2071.

624 19. Kalfaoglu B, et al. T-cell dysregulation in COVID-19. *Biochem. Biophys. Res. Commun.*  
625 2021;538:204–210.

626 20. Meckiff BJ, et al. Imbalance of Regulatory and Cytotoxic SARS-CoV-2-Reactive CD4<sup>+</sup> T  
627 Cells in COVID-19. *Cell* 2020;183(5):1340-1353.e16.

628 21. Henrickson SE, et al. Antigen Availability Determines CD8<sup>+</sup> T Cell-Dendritic Cell  
629 Interaction Kinetics and Memory Fate Decisions. *Immunity* 2013;39(3):496–507.

630 22. Flynn JK, Gorry PR. Stem memory T cells (TSCM)—their role in cancer and HIV  
631 immunotherapies. *Transl. Immunol.* 2014 3, e20; doi:10.1038/cti.2014.16

632 23. Masopust D, Schenkel JM. The integration of T cell migration, differentiation and  
633 function. *Nat. Rev. Immunol.* 2013;13(5):309–320.

634 24. Bellesi S, et al. Increased CD95 (Fas) and PD-1 expression in peripheral blood T  
635 lymphocytes in COVID-19 patients. *Br. J. Haematol.* 2020;191(2):207–211.

636 25. Vardhana SA, Wolchok JD. The many faces of the anti-COVID immune response. *J. Exp.*  
637 *Med.* 2020;217(6). doi:10.1084/jem.20200678

638 26. Zheng M, et al. Functional exhaustion of antiviral lymphocytes in COVID-19 patients.  
639 *Cell. Mol. Immunol.* 2020;17(5):533–535.

640 27. Kared H, et al. SARS-CoV-2–specific CD8<sup>+</sup> T cell responses in convalescent COVID-19  
641 individuals. *J. Clin. Invest.* 2021;131(5):e145476.

642 28. Mullins IM, et al. CXCR3 Chemokine Receptor 3 Expression by Activated CD8<sup>+</sup> T cells Is  
643 Associated with Survival in Melanoma Patients with Stage III Disease. *Cancer Res.*  
644 2004;64(21):7697–7701.

645 29. Laing AG, et al. A dynamic COVID-19 immune signature includes associations with poor  
646 prognosis. *Nat. Med.* 2020;26(10):1623–1635.

647 30. Fuertes Marraco SA, et al. Long-lasting stem cell–like memory CD8<sup>+</sup> T cells with a  
648 naïve-like profile upon yellow fever vaccination. *Sci. Transl. Med.* 2015;7(282):282ra48-  
649 282ra48.

650 31. Gao S, et al. Stem cell-like memory T cells: A perspective from the dark side. *Cell.*  
651 *Immunol.* 2021;361:104273.



652 32. Connors TJ, et al. Airway CD8<sup>+</sup> T Cells Are Associated with Lung Injury during Infant  
653 Viral Respiratory Tract Infection. *Am. J. Respir. Cell Mol. Biol.* 2016;54(6):822–830.

654 33. Britton WJ. CXCR6-Deficiency Improves the Control of Pulmonary Mycobacterium  
655 tuberculosis and Influenza Infection Independent of T-Lymphocyte Recruitment to the Lungs.  
656 *Front. Immunol.* 2019;10:16.

657 34. Gattinoni L, et al. A human memory T cell subset with stem cell-like properties. *Nat.*  
658 *Med.* 2011;17(10):1290–1297.

659 35. Mylvaganam GH, et al. Dynamics of SIV-specific CXCR5<sup>+</sup> CD8 T cells during chronic  
660 SIV infection. *Proc. Natl. Acad. Sci.* 2017;114(8):1976–1981.

661 36. Cieri N, et al. IL-7 and IL-15 instruct the generation of human memory stem T cells from  
662 naive precursors. *Blood* 2013;121(4):573–584.

663 37. Lugli E, et al. Identification, isolation and in vitro expansion of human and nonhuman  
664 primate T stem cell memory cells. *Nat. Protoc.* 2013;8(1):33–42.

665 38. Sant AJ, McMichael A. Revealing the role of CD4<sup>+</sup> T cells in viral immunity 209(8):5.

666 39. Robson B. Computers and viral diseases. Preliminary bioinformatics studies on the design  
667 of a synthetic vaccine and a preventative peptidomimetic antagonist against the SARS-CoV-2  
668 (2019-nCoV, COVID-19) coronavirus. *Comput. Biol. Med.* 2020;119:103670.

669 40. Dutta NK, et al. The Nucleocapsid Protein of SARS-CoV-2: a Target for Vaccine  
670 Development. *J. Virol.* 2020;94(13):e00647-20, /jvi/94/13/JVI.00647-20.atom.

671 41. Grifoni A, et al. A Sequence Homology and Bioinformatic Approach Can Predict  
672 Candidate Targets for Immune Responses to SARS-CoV-2. *Cell Host Microbe*  
673 2020;27(4):671-680.e2.

674 42. Tang JW. Emergence of a new SARS-CoV-2 variant in the UK. *J. Infect.* in press:1–2.

675 43. Mudumba S, et al. Photonic ring resonance is a versatile platform for performing  
676 multiplex immunoassays in real time. *J. Immunol. Methods* 2017;448:34–43.

677 44. Miyara M, et al. Detection in whole blood of autoantibodies for the diagnosis of  
678 connective tissue diseases in near patient testing condition. *PLOS ONE* 2018;13(8):e0202736.

679  
680



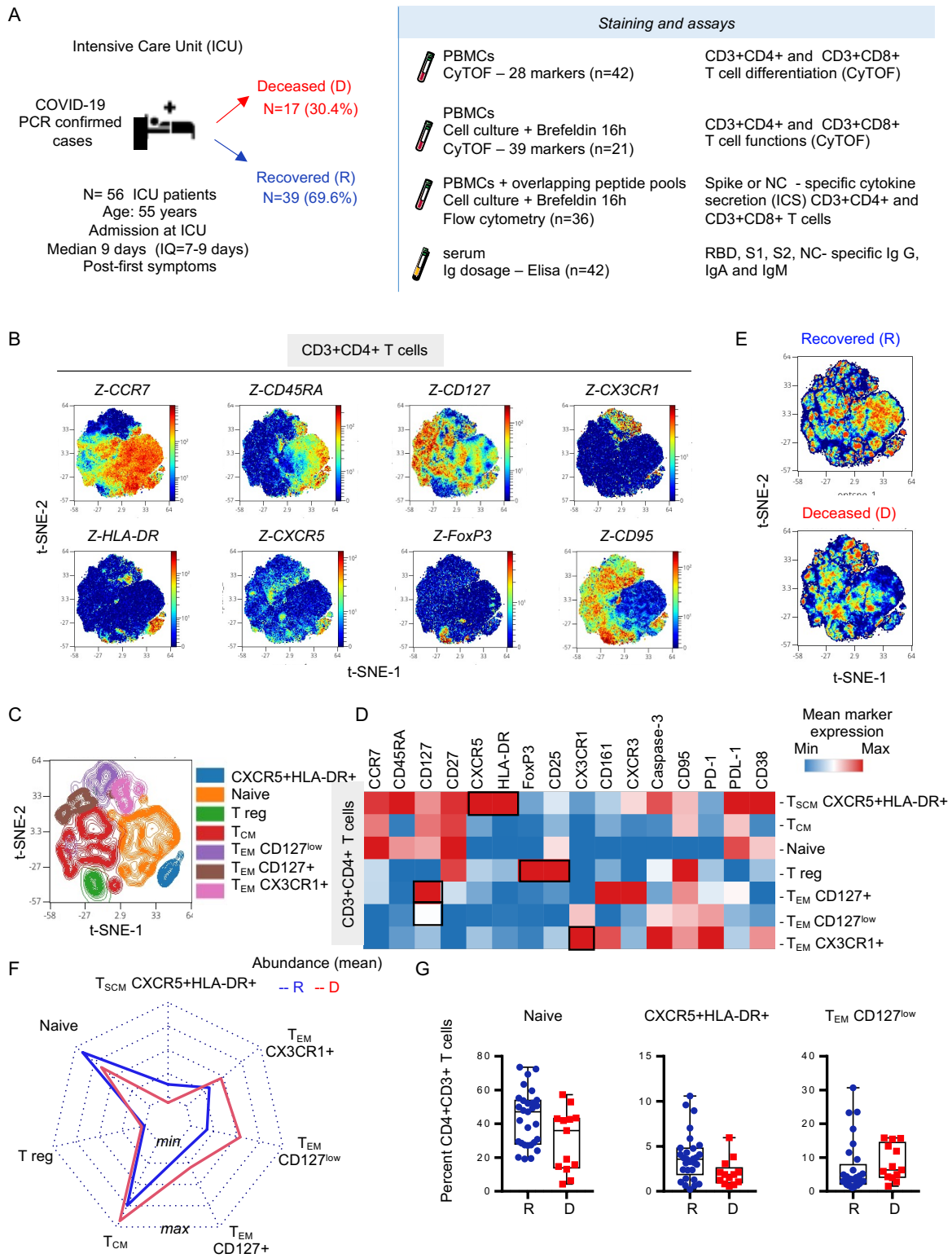
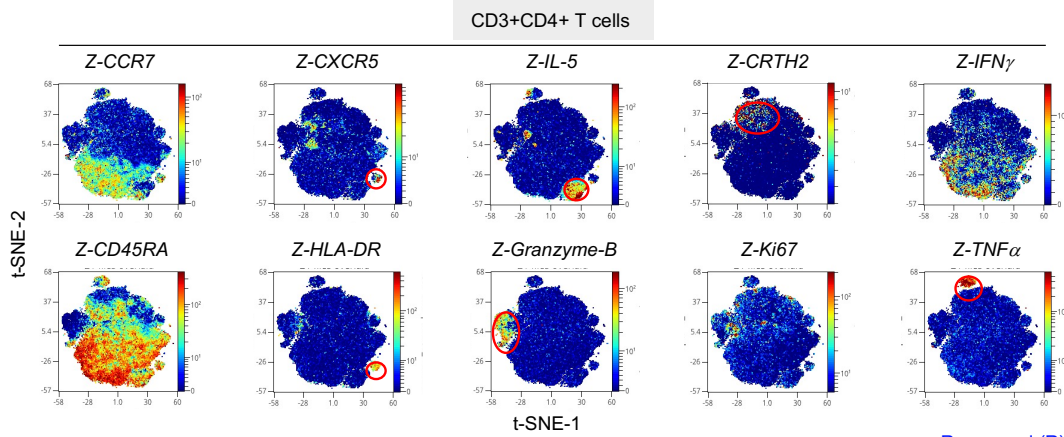


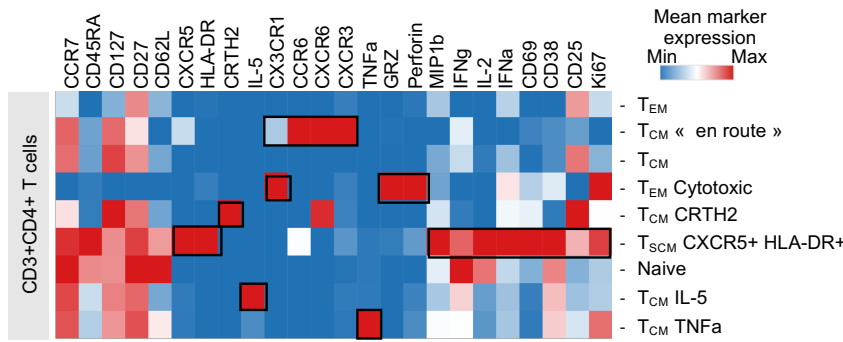
Figure 1

686 **Figure 1: Increased CXCR5+HLADR+ CD4+ T cells and decreased T<sub>EM</sub> subsets outlines**  
687 **critical SARS-CoV-2 infection survival. A)** Fifty-six patients with confirmed SARS-CoV-2  
688 infection were admitted in ICU at a median of 9 days post symptoms. PBMC samples were  
689 collected to assess T cell phenotypes (n=42, recovered= 29, deceased=13) and expression of  
690 effector molecules (n=21, recovered= 12, deceased=9) using mass cytometry panel #1 and  
691 panel #2 (Supplementary Table S1 and S2, respectively). SARS-CoV-2 peptide-specific  
692 cytokine-producing T cells were analyzed by flow cytometry (S1, S2 n=46 (31 recovered and  
693 15 deceased patients; NC n=39 (28 recovered and 11 deceased). Humoral responses were  
694 measured in the serum (n=42, recovered= 29, deceased=13). CD3+CD4+ T cell (50.000  
695 events) were randomly taken among sample for unsupervised cluster using FlowSOM. **B)**  
696 Density plot t-SNE representing the expression of indicated markers. **C)** Spatial t-SNE  
697 representing 7 major clusters as indicated. **D)** Heatmap representation of mean signal intensity  
698 of each marker in identified CD3+CD4+T cell populations. **E)** Density plot t-SNE  
699 representing abundance of events using concatenated files of 29 recovered (R) and 13  
700 deceased (D) patients. **F)** Radar representing mean (min/max normalized) abundance of  
701 CD3+CD4+T cell subsets in 29 recovered (R, blue) and 13 deceased (D, red) patients. **G)** Box  
702 and whisker plots with min and max of CD3+CD4+T cell subset abundances in 29 recovered  
703 (R, blue) and 13 deceased (D, red) patients. All points are shown. Multiple Mann-Whitney  
704 test using Benjamini, Krieger, and Yekutieli FDR correction was performed with significance  
705 set at *q-value* < 0.05.  
706

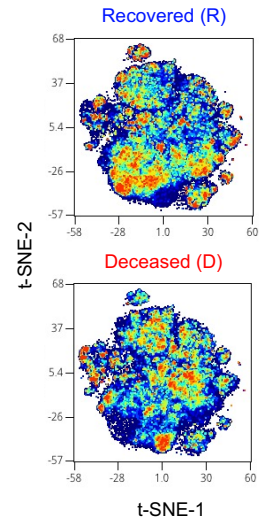
A



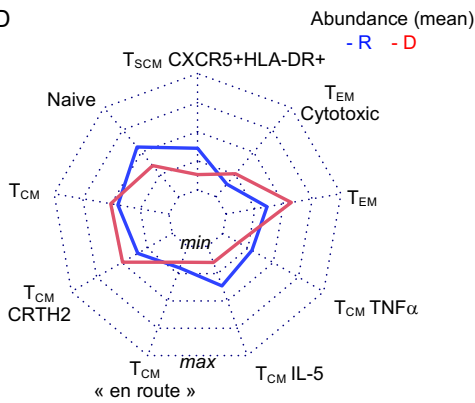
B



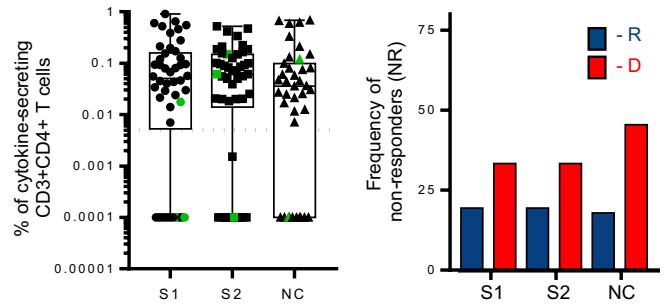
C



D



E



F

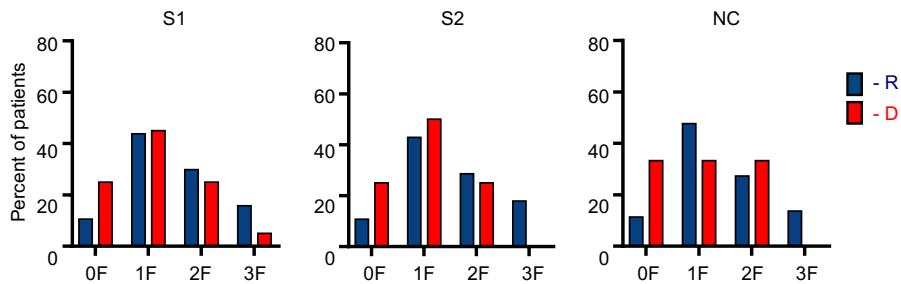


Figure 2

712 **Figure 2: Increased frequencies of circulating polyfunctional CXCR5+HLADR+ CD4+**  
713 **T cells and T<sub>EM</sub> subsets are associated with survival critically infected COVID-19**  
714 **patients.** PBMCs from 21 critical COVID-19 patients were incubated with brefeldin A (16  
715 hours) and stained using multiparametric mass cytometry panel #2 (n=21, recovered (R)= 12,  
716 deceased (D)=9). **A)** CD3+CD4+ T cells (20.000 subsampling events) were randomly taken  
717 for unsupervised cluster using FlowSOM. Density plot t-SNE represents the expression of  
718 indicated markers. **B)** Heatmap representation of mean signal intensity of each marker in  
719 CD3+CD4+T cells. **C)** Density plot t-SNE representing abundance of events using  
720 concatenated files of 12 recovered (R) and 9 deceased (D) patients. **D)** Radar representing  
721 mean (min/max normalized) abundances of CD3+CD4+ T cell subsets in 12 R (blue) and 9 D  
722 (red) patients. Multiple Mann-Whitney test using Benjamini, Krieger, and Yekutieli False  
723 discovery rate (FDR) correction was performed with significance set at *q-value* < 0.05.. **E)**  
724 SARS-CoV-2 specific T cell responses were measured in PBMC from 46 ICU patients at day  
725 15 ± 0.85 (mean ± SEM) post-symptoms onset. PBMCs were stimulated for 16 h with SARS-  
726 COV-2 overlapping peptides: S1, S2 and NC. The frequency of specific CD4+T cells  
727 (boolean gating of IFN $\gamma$ , IL2, and TNF $\alpha$ ) is represented with box and whiskers (min to max)  
728 after background subtraction according to background control (left panel). The frequency of  
729 non-responders (with <0.005% cytokine-secreting CD3+CD4+ T cells) is represented among  
730 recovered (blue; S1 and S2 n=31; NC n= 28) and deceased (red; S1 and S2 n=15; NC n=11)  
731 patients (right panel). **F)** Frequency of patients with cells producing cytokines (0, 1, 2, 3  
732 functions (F)) after stimulation in recovered (blue) and deceased patients (red). Chi2-test did  
733 not show any significancy.

734

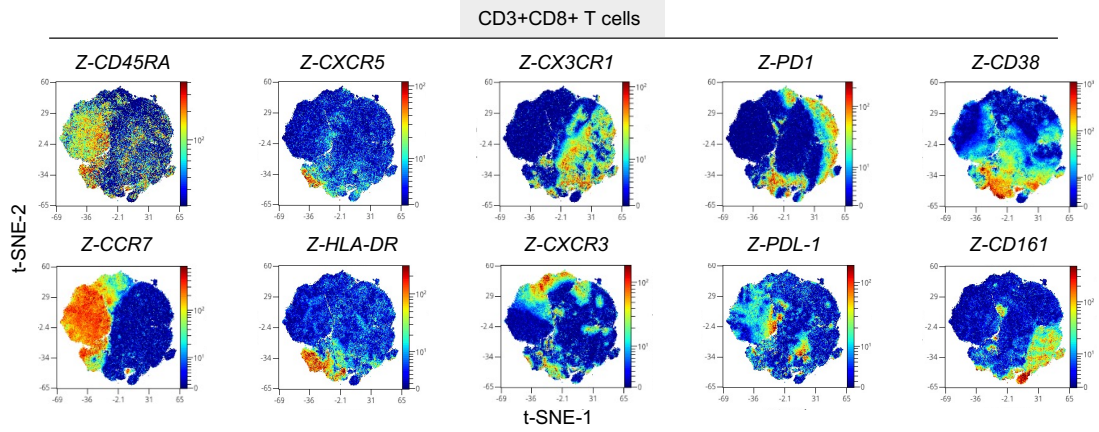
735

736

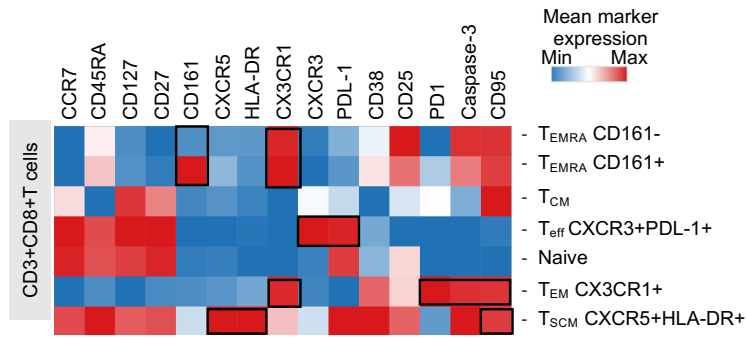
737

738

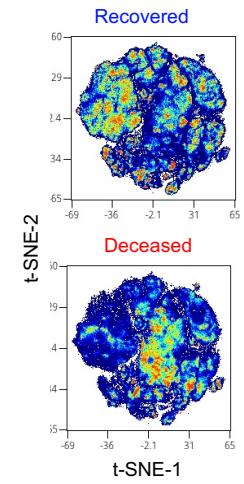
A



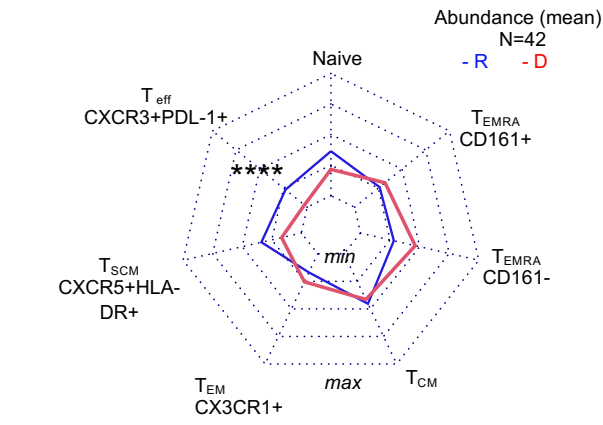
B



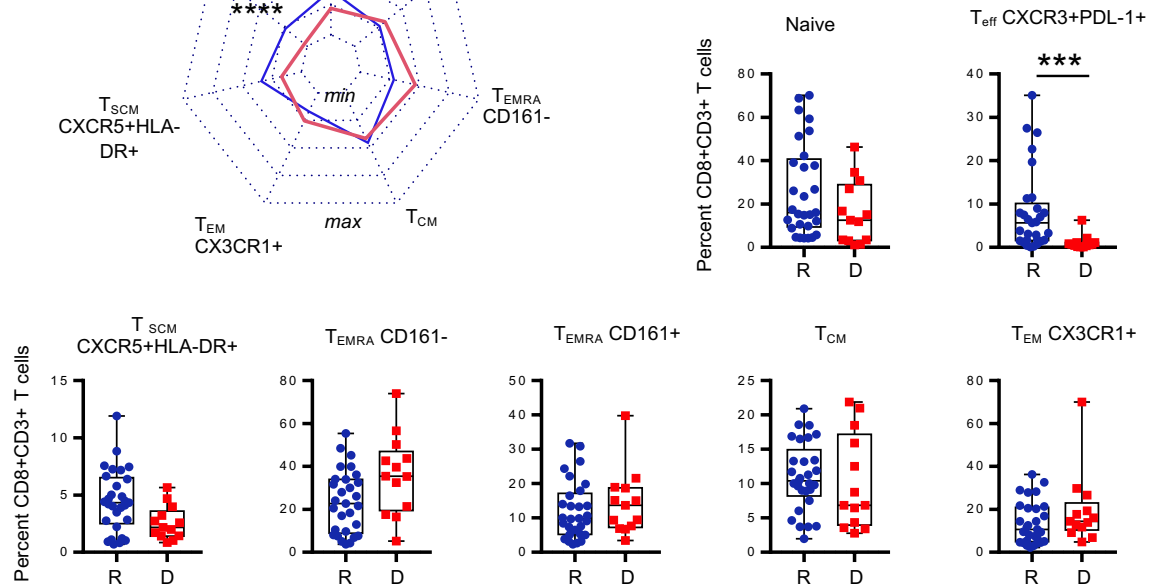
C



D



E



739

740

741

Figure 3

742 **Figure 3: Surviving COVID-19 patients have increased levels of PDL-1+CXCR3+ CD8+**  
743 **T<sub>eff</sub> and CXCR5+HLADR+ CD8+ T<sub>SCM</sub>.**  
744 PBMC samples were collected to assess T cell phenotypes (n=42, recovered= 29,  
745 deceased=13) using mass cytometry panel #1 (Supplementary Table S1). CD3+CD8+ T cells  
746 (50.000 events) were randomly taken among sample for unsupervised cluster using  
747 FlowSOM. **A)** Density plot tSNE representing the expression of indicated markers. **B)**  
748 Heatmap representation of mean signal intensity of each marker in identified CD3+CD8+T  
749 cell population. **C)** Density plot t-SNE representing abundance of events using concatenated  
750 files of 29 recovered (R) and 13 deceased (D) patients. **D)** Radar representing mean (min/max  
751 normalized) abundance of CD3+CD8+T cell subsets in 29 recovered (R, blue) and 13  
752 deceased (D, red) patients. **E)** Box and whisker plots with min and max of CD3+CD8+T cell  
753 subset abundances in 29 recovered (R, blue) and 13 deceased (D, red) patients. All points are  
754 shown. Multiple Mann-Whitney test using Benjamini, Krieger, and Yekutieli False discovery  
755 rate (FDR) correction \*\*\* *p-value* <0.001.

756

757

758

759

760

761

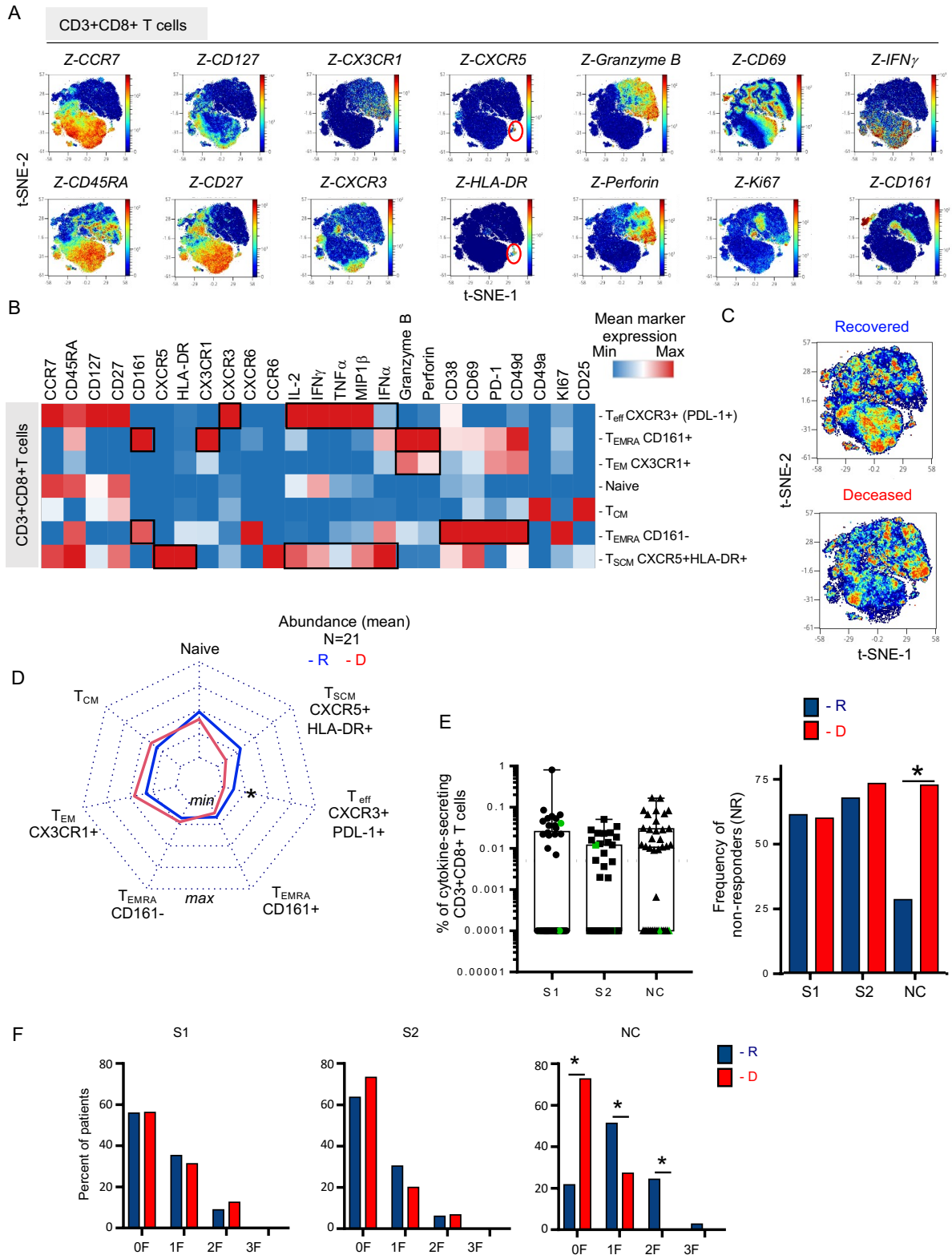


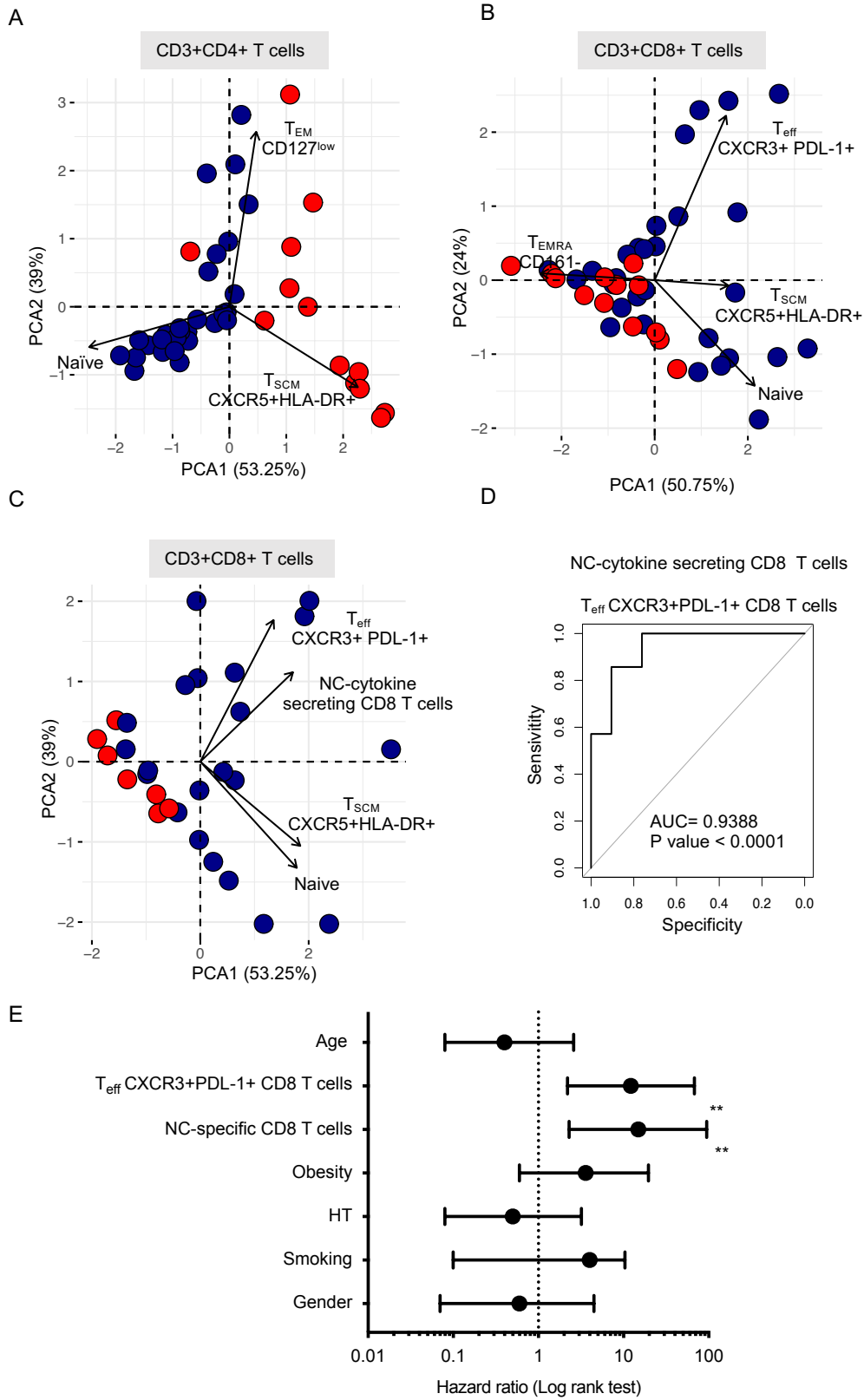
Figure 4

762  
763  
764  
765



766 **Figure 4: Abundance of polyfunctional PDL-1+CXCR3+ CD8+ T cells and**  
767 **Nucleoscapid-specific cytokine-producing T cells define survival versus fatal outcome**  
768 **following critical SARS-CoV-2 infection.** PBMCs from critical COVID-19 patients were  
769 incubated with brefeldin A (16 hours) and stained using multiparametric mass cytometry  
770 panel #2 (n=21, recovered= 12, deceased=9). **A)** CD3+CD8+ T cell (20.000 events) were  
771 randomly taken among sample for unsupervised cluster using FlowSOM. Density plot t-SNE  
772 representing the expression of indicated markers. **B)** Heatmap representation of mean signal  
773 intensity of each marker in CD3+CD8+T cell subsets. **C)** Density plot t-SNE representing  
774 abundance of events using concatenated files of 12 recovered (R) and 9 deceased (D) patients.  
775 **F)** Radar representing mean (min/max normalized) abundances of CD3+CD4+T cell subsets  
776 in 12 R (blue) and 9 D (red) patients. Multiple Mann-Whitney test using Benjamini, Krieger,  
777 and Yekutieli False discovery rate (FDR) correction with significance set at adjusted p-  
778 value<0.05. **E)** SARS-CoV-2 specific T cell responses were measured in PBMC from 46 ICU  
779 patients at day 15 ± 0.85 (mean ± SEM) post-symptoms onset. PBMCs were stimulated for 16  
780 h with SARS-COV-2 overlapping 15mer-peptides (S1, S2 and NC). The frequency of specific  
781 CD8+T cells (boolean gating of IFN $\gamma$ , IL2, and/ TNF $\alpha$ ) is represented with box and whiskers  
782 (min-to-max) after background subtraction according to background control (left panel).  
783 Color-code (green) symbols represent individuals that were under immunosuppressive  
784 treatment when SARS-CoV-2 specific responses were studied. Individuals were considered  
785 responders when the frequency of cytokines produced was >0.005% of CD3+CD8+ cells. The  
786 frequency of non-responders is represented among recovered (blue, S1 and S2: n=31; NC n=  
787 28) and deceased (red, S1 and S2 n=15; NC n=11) patients (right panel). Chi2-test  
788 significance was set at \* *p-value* < 0.05. **F)** Frequency of patients with detectable cells  
789 producing cytokines (0, 1, 2, 3 functions (F)) after stimulation in recovered (blue) and  
790 deceased patients (red). Chi2 test significance was set at \* *p-value* < 0.05.  
791





792  
793  
794  
795

Figure 5

796 **Figure 5: Principal Component Analysis of T cell frequencies discriminate survival and**  
797 **decreased ICU patients following critical SARS-CoV2 infection.** Principal component  
798 analysis (PCA) representations (R software) : **A)** CD4+ T-cell subset abundance and **B)** CD8+  
799 T-cell subset abundance as indicated, **C)** CD8+ T-cell subsets as indicated and frequency of  
800 NC-specific CD8+ T-cells. Color code indicate patients who recovered (blue) and patients  
801 who deceased (red). **D)** Receiver Operating Characteristic (ROC) curve (R software)  
802 modeling the abundance of PD-L1+CXCR3+ T<sub>eff</sub>-cells and NC-specific CD8+ T-cells in  
803 disease survival or death outcomes. Area under the curve (AUC) = 0.9388, *p-value* < 0.001.  
804 **E)** Forest plots comparing hazard ratio (Mantel-Haenszel) for death in 28 patients according  
805 abundance of PD-L1+CXCR3+ T<sub>eff</sub>-cells and NC-specific CD8+ T-cells. Log-rank (Mantel-  
806 Cox) test was used to compare HR between groups, with significance defined by a **\*\*p-value**  
807 **< 0.001.**  
808

809 **Table 1: Demographics and baseline characteristics of 56 patients with COVID-19 in**  
 810 **Intensive Care Unit (ICU)**

<b>All patients (N=56)</b>	
Men	43 (76.8)
Age, years, median (IQR)	55 (48 – 62)
<b>Chronic medical illness</b>	
Heart disease	4 (7.1)
<i>Body mass index (kg/m<sup>2</sup>)</i>	
Normal (18.5-25)	6 (10.7)
Overweight (25-30)	23 (41.1)
Obesity (≥30)	27 (48.2)
Hypertension	27 (48.2)
Immunocompromised*	4 (7.1)
<i>Smoking habits</i>	
Never smoker	50 (89.3)
Former smoker	6 (10.7)
<b>Treatment regimen at baseline</b>	
Long-term immunosuppressive agent use	4 (7.1)
Corticosteroids	3 (5.4)
<b>Severity score at baseline</b>	
SAPS II, median (IQR)	39 (29 - 52)
<b>Time from onset of symptoms to admission</b>	
Days, median (IQR)	9 (7 – 12)
<b>Laboratory findings at baseline</b>	
Neutrophil count, x10 <sup>9</sup> /L, median (IQR) [range : 2.7 – 5]	10.05 (6.32 – 13.14)
Lymphocyte count, x10 <sup>9</sup> /L, median (IQR) [range: 1.5 – 4]	0.88 (0.61 – 1.15)
<b>Chest CT finding: extension of GGO and/or consolidation<sup>‡</sup></b>	
<25%	0 (0)
25-50%	5 (38.5)
50-75%	3 (23.1)
> 75%	5 (38.5)
<b>Treatment</b>	
<i>Hydroxychloroquine</i>	27 (48.2)
<i>Glucocorticoids</i>	5 (8.9)
<i>Tocilizumab or sarilumab</i>	7 (12.5)
<i>Remdesivir</i>	3 (5.2)
<i>Lopinavir/ritonavir</i>	5 (8.9)
<i>Antibiotic therapy</i>	52 (92.9)
<i>Oxygen therapy</i>	56 (100)
Invasive mechanical ventilation	50 (89.3)
<i>Extracorporeal membrane oxygenation</i>	29 (51.8)
<i>Haemodialysis</i>	21 (28.9)
<b>Complications</b>	
Acute respiratory distress syndrome	51 (91.1)
Acquired mechanical ventilation pneumonia	38 (67.9)
<b>Clinical outcome<sup>†</sup></b>	
Duration of hospitalization, median (IQR)	25 (10 – 50)
Discharged	39 (69.6)
Deceased	17 (30.4)

811 Values are expressed as n (%), unless stated otherwise.

812 \*including cardiac, liver or kidney allograft, hematopoietic stem cell transplantation  
813 □ 13 patients were assessed  
814 † As of December 2nd, 2020  
815 CT, computed tomography; GGO, ground-glass opacities; SAPS II, Simplified Acute  
816 Physiology Score II  
817  
818  
819